Dynamic Protein−Water Relationships during β-Sheet Formation

Xiao Hu,[†] David Kaplan,[‡] and Peggy Cebe*,[†]

Department of Physics and Astronomy and Departments of Biomedical Engineering and Chemical and Biological Engineering, Tufts University, Medford, Massachusetts 02155

Received July 12, 2007; Revised Manuscript Received March 7, 2008

ABSTRACT: We investigated the polymer−water interaction in a model fibrous protein. *Bombyx mori* silk fibroin film, a typical model of biodegradable material, was cast from aqueous solution and analyzed in this study. Differential scanning calorimetry (DSC), its temperature-modulated variant (TMDSC), and the time-resolved technique of Fourier transform infrared spectroscopy (FTIR) were used for the first time to monitor the detailed structural changes of silk fibroin during heating and during isothermal crystallization above the glass transition temperature, $T_g \sim 451$ K (178 °C). Results show that intermolecular bound water molecules, acting as a plasticizer, will strongly affect the secondary structure of silk fibroin. DSC study shows that silk fibroin initially displays a water-induced glass transition around 80 °C during heating, resulting from a temporary bound water-silk structure. Quantitative thermal analysis of the heat capacity changes of this system during heating revealed that no β-sheet crystals were formed below T_g. FTIR scans also confirmed that no β-sheets were formed during heating and removal of bound water below T_g. During water removal, the amide II region shifts to lower frequency, and the 1515 cm^{-1} band increases slightly, indicating change of the microenvironment in the silk fibroin chains. During isothermal crystallization above T_g, the amide I region of silk fibroin spectra showed a phase transition from the secondary structures of noncrystalline random coils and α-helices to the β-pleated-sheet crystals, while the amide II region and the 1515 cm^{-1} band remain stable during β-sheet formation. Analogy is made between the crystallization of synthetic polymers according to the four-state scheme of Strobl and the crystallization process of silk fibroin, which we suggest proceeds through an intermediate precursor stage associated with water removal. This study provides a deeper understanding of the formation of β-pleated sheets during the crystallization process in silk fibroin, with implications for the crystallization of naturally occurring silk fibers from animals such as the silkworm and spider.

Introduction

The polymer−water interaction remains one of the major challenges in modern macromolecular science. Water molecules affect not only the stability of the macromolecular structure but also the process of their phase transition and crystallization thermodynamics.[1−13] For example, researchers who study food science and protein science must consider the role of bound water molecules.[9,10] In biopolymers, hydration results from different van der Waals, hydrogen bonding, and hydrophobic interactions between water molecules and specific functional groups of the polymers.[8−10] Generally, there are two types of water molecules in studies of polymer−water interactions: the freezing free water and the bound water.[4,5,13] Freezing free water in polymers is unbound water that has the same transition temperature at 273 K (0 °C) as bulk water.[4,5] Bound water is attributed to the strong interaction between water and polymer. One water molecule can be connected by at most four hydrogen bonds (two as acceptor and two as donor) with polymer chains and are held relatively static in the polymer−water system. According to number and stability of bonds, bound water can also be divided into[4,5] freezing and nonfreezing bound water.

Bound water molecules can act as a plasticizer and become incorporated into the polymer structure to increase flexibility, extensibility, and workability of the polymer.[1−13] As a "mobility enhancer", bound water will expand the accessible conformational space of the polymer by decreasing its inter- and intramolecular friction and effective barrier heights for conformational change. Torsional transitions occurring in polymer−water dense systems will result in a new "glass transition". With fluctuation of the torsional barriers, the polymer−water couplings induce changes in the polymer−water system.[10] On the other hand, dehydration will lead the polymer system back to its original glassy state, which implies the loss of long- and intermediate-range diffusion.[4,5,10] Upon heating the polymer−water system to a higher temperature, the energetic barrier that trapped solidlike water molecules will be broken and some bound water molecules will be transformed to become free water molecules. With the water molecules transferring across the polymer molecular layers, a structure transformation will be induced. Water molecules play an important role in the polymer−water system even when the water content is very small and the system is in a solidlike state.

Silk is one of the most interesting biomaterials for the study of the polymer−water interactions.[14,15] As a typical fibrous protein, fibers from *Bombyx mori* (domesticated) silk worm have been used in the textile industry for thousands of years. In the salivary gland of *B. mori* silkworms, silk fibroin exists in the water-soluble silk I form and is spun together with the gluelike sericin into a fiber, leading to the rapid transition to the insoluble conformation (silk II). The phase transitions of silk fibroin have been well studied and reveal the formation of antiparallel β-pleated-sheet crystals during spinning.[1,12,13] On the basis of the sequence of the *B. mori* silk fibroin gene and encoded protein,[16] the highly repetitive GAGAGS region forms the main β-sheet crystalline regions. However, the mechanism of β-sheet crystallization is still unclear. One reason for this uncertainty is that silk fibroin crystallizes rapidly during spinning, making the initial stages of crystallization difficult to study. Exposure of fibroin materials to organic solvents, mechanical stress, high concentration of salts, and thermal treatment induced formation of insoluble β-sheet structure.[6,12,13,17−23] These studies highlight the important role of water in the protein assembly and structural state.

* Corresponding author: Tel 617-627-3365, Fax 617-627-3744, e-mail peggy.cebe@tufts.edu.
[†] Department of Physics and Astronomy.
[‡] Departments of Biomedical Engineering and Chemical and Biological Engineering.

10.1021/ma071551d CCC: $40.75
Published on Web 05/10/2008

In a study of the early stages of solution crystallization of silk fibroin, we have previously reported the important contribution that water makes to the crystallization process of the spun fiber.[13,22] By using SEM, a "micelle" structure was observed before the crystallization of the silk fibers.[22] Among the methods of inducing crystallization of silk fibroin, thermal crystallization provides a wide temperature range to study the structural transitions of the silk fibroin because of the high glass transition temperature (T_g = 451 K (178 °C)[1,13,20,23]) of this protein. Isothermal crystallization of silk fibroin is much slower than in the natural spinning process.[1,13] A recent study showed that aqueous solution-cast silk films contained intermolecular bound water molecules, which could plasticize the silk and cause reduction of the glass transition temperature.[6,13] Using temperature-modulated differential scanning calorimetry (TMDSC), we were able accurately to determine the specific heat capacity of pure amorphous silk fibroin,[13] and a model based on the derived baselines was then used to analyze these water-induced glass transitions at lower temperature.[13] These results predicted that the water-induced glass transitions were not originating from contributions from the β-sheet crystals. Therefore, the conformational changes in the level of protein secondary structure need to be examined in real time during heating.

Fourier transform infrared (FTIR) spectroscopy has become a sensitive tool for determining the structure of biological materials.[24–29] FTIR can serve as a structure-specific probe, and a complete spectrum is available for each time point of measurement.[29–37] Time-resolved FTIR has been used for the study of silk fibroin solution and other protein solutions at different pH values or with added metal ions.[17,38] The process of treating silk nanofibers at different humidity and temperature was observed on a long time scale.[7,39] However, detailed band assignments were not applied. No temperature-related conformational study on cast silk films has been reported. It is necessary to determine temperature effects on silk fibroin and the effects of bound water molecules on secondary structures of the silk protein chains during heating and isothermal holding. This type of study requires a smaller time scale (on the scale of minutes or seconds) and accurate association of spectrum collection with temperature control. With this approach, combined with quantitative heat capacity analysis on silk fibroin films, we can understand the role of water on the mechanism of crystallization in silk fibroin and other similar members of the broader family of fibrous proteins.

Experimental Section

Materials and Preparation. The detailed fibroin preparation process was reported previously.[1,13] Briefly, *B. mori* silkworm cocoons were boiled in Na_2CO_3 aqueous solution to extract sericin. The remaining silk fibroin was dissolved in LiBr solution at 60 °C for 4−6 h and then dialyzed in distilled water using a Slide-a-Lyzer dialysis cassette for 2 days. After centrifugation and filtration to remove insoluble residues, the final 2 wt % silk fibroin aqueous solution was cast in polystyrene Petri dishes to generate silk fibroin films with a thickness of 1−2 μm. Films were placed in a vacuum oven at room temperature for 1 day to remove surface moisture. The films, containing ~5 wt % bound water (measured by thermogravimetric analysis (TGA)[13]), were completely noncrystalline, as shown by FTIR absorption spectroscopy, heat capacity at the glass transition,[1,13] and wide-angle X-ray scattering.

Differential Scanning Calorimetry (DSC). Samples of about 5 mg of fibroin were encapsulated in Al pans and heated in a TA Instruments Q100 DSC with a dry nitrogen gas flow of 50 mL/min. The instrument was calibrated for empty cell baseline and with indium for heat flow and temperature. Standard mode DSC measurements were performed at heating rates of 20, 10, 5, and 2 K/min. Temperature-modulated differential scanning calorimetry (TMDSC) measurements were also performed using a TA Instruments Q100, equipped with a refrigerated cooling system. The silk−water system samples were heated at 5 and 2 K/min with a modulation period of 60 s and temperature amplitudes of 0.796 and 0.318 K, respectively. Aluminum and sapphire reference standards were used for calibration of the heat capacity. The heat capacity measurement consisted of three runs, as described in our earlier work.[1,13,40–44] The same empty Al reference pan was used in all runs, and all Al empty sample pans were kept the same in weight.

From a standard DSC measurement with a constant applied heating rate, q, the total heat capacity consisted of both the reversing and nonreversing components, from

$$mC_p = K''HF/q \tag{1}$$

where K'' is a calibration constant and HF is heat flow. In TMDSC the "reversing heat capacity" was measured, a term representing a heat effect which can be reversed within the temperature range of the modulation and calculated from[13,40–45]

$$|mC_p + C_s - C_r \pm \Delta C_{cell}| = (A_T/A)[(K/\omega)^2 + C_r^2]^{1/2} = K'(A_{HF})/A \tag{2}$$

where m is the initial sample mass, C_p is the specific heat capacity, C_s and C_r are the heat capacity of sample pan and empty reference pan, respectively, and ΔC_{cell} is the cell asymmetry correction.[43,44] A_T is the amplitude of temperature difference between sample and reference, A is the sample temperature modulation amplitude, K is Newton's law calibration constant, independent of modulation frequency ω and reference, A_{HF} is heat flow amplitude, and K' is a calibration constant at each temperature provided the same experimental conditions are maintained to ensure the same heat transfer.

The heat capacity study of polymers and small molecules has been well developed.[2,3,13,46] The heat capacity of the mixed system of amorphous polymer (poly) and small molecules (sm) is based on the evaluation of

$$C_p(\text{poly}-\text{sm}) = C_{vib}(\text{poly}-\text{sm}) + C_{conf}(\text{poly}-\text{sm}) + C_{ext}(\text{poly}-\text{sm}) \tag{3}$$

where C_p(poly−sm) represents the total heat capacity at constant pressure for the system polymer/small molecules, C_{vib}(poly−sm) is the vibrational heat capacity at constant volume, C_{ext}(poly−sm) stands for the external heat capacity, and C_{conf}(poly−sm) denotes the conformational heat capacity. The major part of the total heat capacity comes from vibrational motion. The vibrational heat capacities of the polymer/small molecules system (first term on the right-hand side of eq 3) can be estimated by the addition of C_{vib}(poly) and C_{vib}(sm) according to the equation

$$C_{vib}(\text{poly}-\text{sm}) = X_{poly}C_{vib}(\text{poly}) + X_{sm}C_{vib}(\text{sm}) \tag{4}$$

where X_{poly} and X_{sm} are the weight fractions of polymer and small molecules, respectively.[2,3,13] The calculated mixed vibrational heat capacity for different component fractions can serve as a baseline for the thermal analysis of the mixed heat capacity. The silk−water system is a typical example of this model. The vibrational heat capacity of glassy water has been calculated by Pyda in his study of the starch−water system.[3] The liquid heat capacity of water was calculated by Seki et al.[47] The solid and liquid heat capacity of silk was measured in our previous work.[1,13] To a first approximation, the total heat capacity of the silk−water system at different temperatures is

$$C_p(\text{silk}^{\text{solid}}-\text{water}^{\text{glassy}}) = X_{silk}C_p(\text{silk})^{\text{solid}} + X_{water}C_p(\text{water})^{\text{glassy}} \tag{5a}$$

$$C_p(\text{silk}^{\text{liquid}}-\text{water}^{\text{liquid}}) = X_{silk}C_p(\text{silk})^{\text{liquid}} + X_{water}C_p(\text{water})^{\text{liquid}} \tag{5b}$$

where C_p(silk−water) is the calculated specific heat capacity of the total silk−water system, C_p(silk) and C_p(water) are the

experimental specific heat capacities of silk and water, respectively, X_{silk} is the weight fraction of silk in the system, and X_{water} is the weight fraction of water, with the relationship $X_{silk} = 1 - X_{water}$. Since total mass decreases during heating, the measured heat capacity, C_p (appearing in eqs 1–5), is corrected by the temperature-dependent mass, $M(T)$,[13] and replaced by C_{pm} using

$$C_{pm} = C_p/M(T) \quad (6)$$

Fourier Transform Infrared Spectroscopy (FTIR). The silk fibroin samples were put into an optical microscopy hot stage (Mettler, FP90) as free-standing films (no IR transparent substrate was used) and examined in transmission mode. This hot stage was then placed under the FTIR microscopic spectrometer (Bruker Equinox 55/S) with a liquid nitrogen cooled MCT (mercury cadmium telluride) detector. The analysis was performed in transmission mode using the microscope. Holes in the hot stage platens permitted the IR beam to pass through the samples directly. The temperature in the heating holder was monitored with the central processor of the hot stage and was calibrated with a thermocouple before the experiments. The position and focus of the samples were adjusted microscopically through an aperture in the IR optical system. The aperture used to give the best signal-to-noise ratio was 10 mm.

For each measurement, 1 min scans were coadded and Fourier transformed employing a Genzel−Happ apodization function to yield spectra with a nominal resolution of 4 cm^{-1}. The frequency ranged from 400 to 4000 cm^{-1}. To identify silk secondary structures from the absorption spectra, we obtained the positions of the absorption band maxima from Fourier self-deconvolution[1,24,25] performed by using the Opus 5.0 software as described previously.[1] All figures presented in this work show only raw (unsmoothed) absorption data, corrected by background subtraction. To obtain good signal-to-noise ratio, relatively thin silk films (1−2 μm) were prepared by casting a smaller volume of silk solution on the polystyrene dish. This relatively thin film had no difference in secondary structure when compared with the thicker films, based on DSC and X-ray. A control sample, of silk fibroin crystallized by exposure to MeOH, was used to check the effects of temperature and isothermal holding time on a sample whose structure was unchanging during the heating and isothermal crystallization. The absorbance value of the MeOH-treated control film was comparable to that of the untreated sample film.

Results and Discussion

Thermal Analysis. Figure 1 shows standard DSC scans of silk fibroin films with heating rates (a) 20, (b) 10, (c) 5, (d) 2, and (e) 2 K/min after annealing, from −65 to 280 °C. The samples from (a) to (d) are silk fibroin films containing about 5.5 wt % bound water molecules before heating, which was verified by TGA at different heating rates and has proven to be a typical bound water content in the aqueous solution cast silk fibroin films.[13] The sample in (e) was pure silk fibroin as a reference sample, which was first treated below the glass transition temperature of the pure silk fibroin by repeated "thermal cycles" and has been reported in detail in our previous work.[1,13] The pure sample in (e) showed the glass transition of pure silk fibroin at around $T_g(2) = 178$ °C and a nonisothermal crystallization peak(2) at around 213 °C. After the appearance of the crystallization peak, at around 230 °C the film immediately started to degrade, with endotherm peak at around 260 °C. There were no endothermic or exothermal events before the glass transition temperature $T_g(2)$ for the pure silk fibroin samples which contained no bound water molecules. The silk fibroin samples containing bound water in (a)−(d) showed a difference in thermal properties compared with the dried sample (e). A new series of additional glass transitions, $T_g(1)$, were formed at around 80 °C in all these samples, and a slight increase of $T_g(1)$ was observed for the samples heated more rapidly.

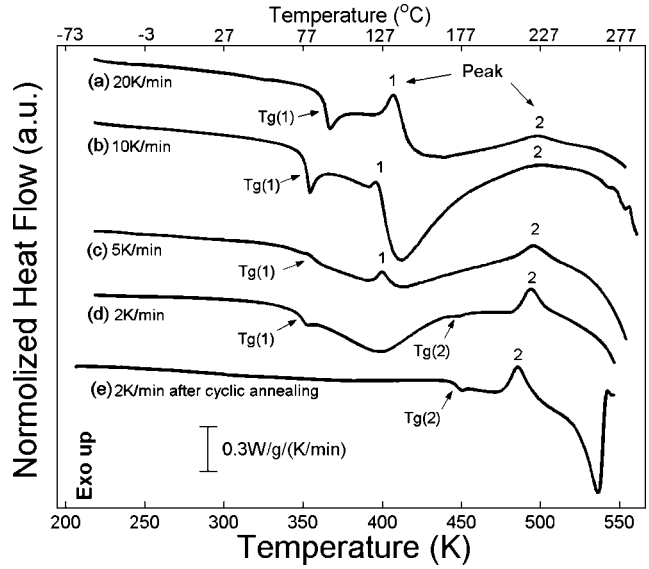

Figure 1. Standard DSC scans of silk fibroin films from −65 to 280 °C with the heating rates (a) 20, (b) 10, (c) 5, (d) 2, and (e) 2 K/min. The samples from (a) to (d) are silk fibroin films containing 5.5 wt % bound water molecules before heating. The sample in (e) is a totally pure silk fibroin sample after water removal. The heat flow has been normalized for sample mass and for heating rate.

A series of low-temperature exothermal peaks(1) were also formed when higher heating rates were used (a−c). With a reduction in heating rate, the new exothermal peak was smaller and finally was not observed in sample (d). A large endotherm always appeared in the temperature region from 80 to 150 °C. In samples (a) and (b) heated more quickly, water removal endotherms occurred after the first exothermal peaks(1). But in the samples heated more slowly (c, d), these endotherms almost covered the entire region of the first glass transitions ($T_g(1)$) and the first exothermal peak(1). After these huge endothermic peaks, the glass transition of the pure silk fibroin occurred at around $T_g(2) = 178$ °C and clearly appeared in sample (d).

The nonisothermal crystallization peaks(2) for pure silk fibroin were also observed in all samples (a) to (d), and they had slightly shifted to higher temperature for the samples heated more quickly. After the crystallization peaks(2), all samples started to degrade, but the degradation temperatures were a little higher than that of pure silk fibroin (e). The tiny annealing endothermic peaks in both the $T_g(1)$ and $T_g(2)$ regions were due to the physical aging effect of the samples[13] as they had been annealed at room temperature in a vacuum oven for 1 day to remove unbound water. Therefore, no melting peaks for the freezing free water were observed around 0 °C in any of the silk samples. It was clear that all these new features before the $T_g(2)$ in samples (a) to (d) were due to the effect of the bound water molecules in the silk fibroin structure.

The origin of the large endothermic peak, ranging from 80 to 150 °C, has been a topic of discussion for many years.[6,8,20] Some authors believed that this peak was directly contributed by the melting of bound water in the silk fibroin samples.[8] They furthermore use this "melting peak" to calculate the entropy of the bound water in their silk fibroin samples. Other authors pointed out that this peak is just the experimental sign of the water loss, which means that the water inside the silk fibroin absorbed heat energy and finally evaporated from the structure of the silk samples at a high temperature, around 150 °C.[20] However, these discussions did not consider the effect of the heating rate on this endothermic peak. Observation of the low temperature glass transition, $T_g(1)$, followed by a crystallization-like exothermal peak(1), as observed in the present study,

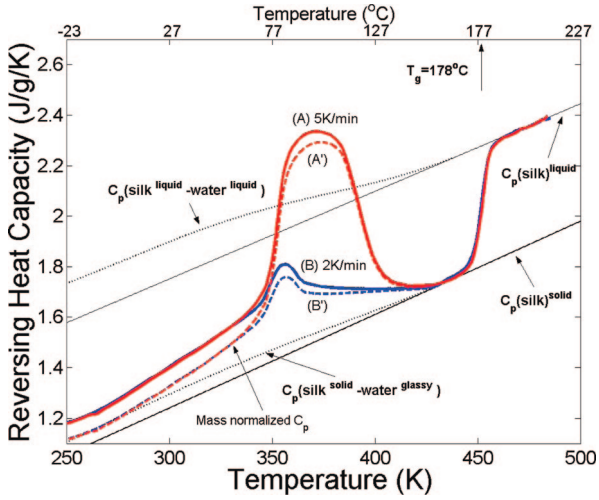

Figure 2. Specific reversing heat capacity of silk fibroin samples measured by TMDSC. The silk fibroin samples contain 5.5 wt % bound water molecules. Curve (A) is from sample heated with a rate of 5 K/min, modulated with temperature amplitude of 0.796 K and period of 1 min; Curve (B) is from sample heated with a rate of 2 K/min, modulated with temperature amplitude of 0.318 K and period of 1 min. Curves (A′) and (B′) (dashed lines) reflect the mass-revised heat capacity of samples (A) and (B), respectively, derived from eq 6. The solid lines are the calculated baseline heat capacities of the liquid and solid states of pure dried silk. The dotted lines are the calculated baseline heat capacities of the liquid and solid states of the silk and water system.

complicates the situation. With a reduction of the heating rate, the exothermal peaks (1) for the water−silk system become less obvious. They were gradually buried in the large endothermic peaks. However, the glass transition of the silk−water system, $T_g(1)$, can still be observed in all water-containing samples. In the silk samples (a) and (b) heated more quickly, the large endothermic peaks followed after the first exothermal peaks (1), which indicates that they have the property of a "melting" peak. However, the first exothermal peak (1), in the sample (c) heated at lower rates, almost appeared at the center of the large endothermic peak. Since melting cannot occur before crystallization, the large endothermic peak is related to water evaporation. We have observed the water loss by TGA in our previous work.[13] Therefore, we can confirm that this endothermic peak must arise from the heat of vaporization for the bound water molecules when leaving the silk structure. However, standard DSC cannot reveal whether or not part of the heat in this endothermic peak also contributes to a "melting" process.

To reveal whether a "melting" process was hiding in this large endothermic water peak and the meaning of the exothermal peak (1), we must exclude the effect of the heat during water evaporation. Fortunately, modern TMDSC provides a method to address this problem. By providing a small modulated temperature during the normal heat ramping process, the reversing heat flow of the silk samples can be separated from the nonreversing heat flow.[1,13,40–45] As the water evaporation is a typical nonreversing thermal process, we can obtain direct information from this process about whether a "melting" event has happened after the exothermal peak (1) for the silk−water system.

Figure 2 shows the specific reversing heat capacities of the silk fibroin samples measured by TMDSC. Samples were the same as those used for the DSC study and contained 5.5 wt % bound water. Sample (A) was heated at a rate of 5 K/min, with $A = 0.796$ K and period of 1 min; Sample (B) was heated at a rate of 2 K/min, with $A = 0.318$ K and period of 1 min. The samples are not shown after heating at 20 and 10 K/min, but the features were similar to the samples heated with slower rates in the water−polymer system.

The constant mass after water removal was used to normalize the heat capacities of samples (A) and (B). In our previous study,[13] the heat capacity of the pure silk fibroin (sample (e) in Figure 1) was analyzed and solid and liquid heat capacities of pure silk fibroin were measured using standard DSC, TMDSC, and quasi-isothermal TMDSC. These heat capacities were used to quantitatively construct the underlying baseline heat capacity for the combined silk−water system. Furthermore, a theoretical model based on eqs 2−5 was built to study the heat capacity of the silk−water system. The measured heat capacity of the silk samples in the temperature region −50 to 80 °C was compatible with the model in the low-temperature regime. In the higher temperature region (80−140 °C) above the glass transition $T_g(1)$ of the silk−water system, the model did not fit the data.

By combining information from the higher temperature region and the different heating rates in this study, we can explore the whole picture concerning effects of water on the crystallization of silk fibroin. Figure 2 also includes four baselines. The two long baselines (in solid lines), marked as $C_p(\text{silk})^{\text{solid}}$ and $C_p(\text{silk})^{\text{liquid}}$, come from the solid (lower) and liquid (upper) heat capacities, respectively, of the pure silk fibroin. These two baselines are the result of the DSC data acquired by the method "repeated thermal cycles" in our previous work and were verified by other methods like quasi-isothermal TMDSC.[13] There was no experimental way to obtain the heat capacity of the pure "liquidlike" silk fibroin structure directly when in the bound water-containing state. Fortunately, we can quantitatively compare the heat capacity of the pure silk fibroin in these two different noncrystalline states by the model previously derived.[1,13]

For this purpose, two short baselines (dotted lines) based on eq 5 were drawn in Figure 2. The solid silk−water baseline, labeled $C_p(\text{silk}^{\text{solid}}-\text{water}^{\text{solid}})$, was based on the combination of the heat capacity of the glassy water and the solid "dense" silk fibroin by weight fraction at different temperatures. The liquid silk−water baseline, labeled $C_p(\text{silk}^{\text{liquid}}-\text{water}^{\text{liquid}})$, was based on the combination of heat capacities of liquid water and liquid silk fibroin by weight fraction at different temperatures. Both samples have higher heat capacity values in the low-temperature region compared with the heat capacity values of pure silk fibroin, but they end at the same values as the pure silk fibroin when the water molecules have all finally left the system at a specific temperature around 160 °C. The weight fraction functions were obtained from curve fitting of the TGA data where samples were measured under the same experimental conditions.[13]

Curves (A′) and (B′) in Figure 2 are the mass revised heat capacities of samples (A) and (B), respectively, derived from eq 6. The mass changing function was obtained directly from TGA under the same experimental conditions. At temperatures below −15 °C, the experimental heat capacities of the silk−water system in (A′) and (B′) start to match the solid silk−water baseline very closely. In the temperature region from 80 to 160 °C, a clear glass transition, $T_g(1)$, was formed in both samples (A) and (B). The slowly heated sample (B) has a lower heat capacity change compared with the quickly heated sample (A), which may result from the easier water loss in the slowly heated samples. However, neither graphic (A′) nor (B′) obeyed the liquid baselines we derived from the pure liquid silk and liquid water in the vicinity of $T_g(1)$. The heat capacity of sample (A) heated at 5 K/min is higher than the liquid baseline even after mass correction to (A′), but the heat capacity of sample (B) heated at 2 K/min is lower than the liquid baseline after mass correction to (B′). We therefore can conclude that the heat

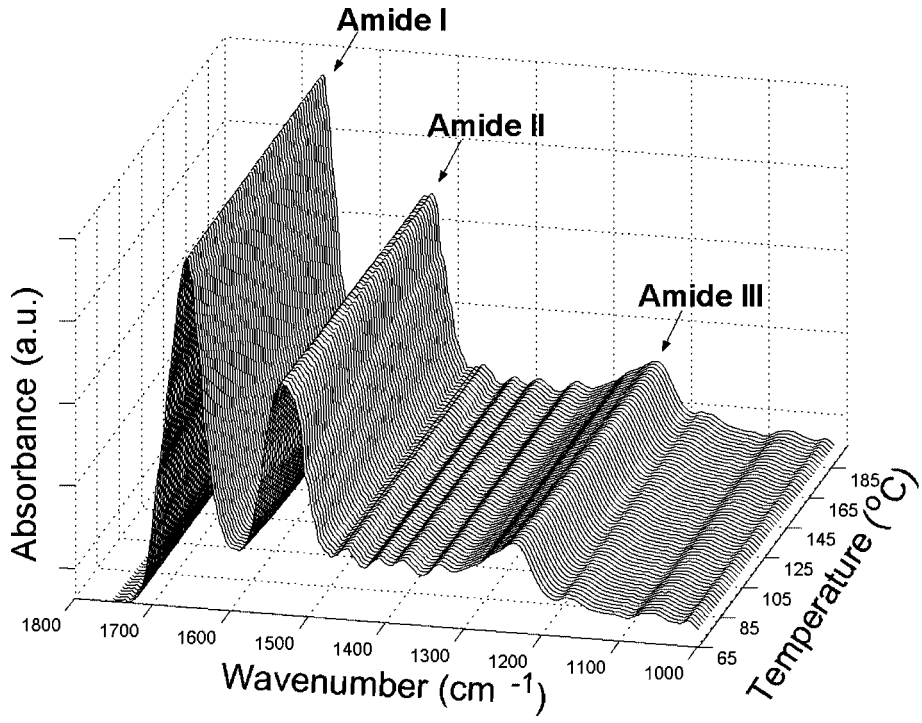

Figure 3. Typical FTIR spectra during heating from 65 to 165 °C at a heating rate of 2 K/min. The collection time for each spectrum is 63 s. The frequency is shown from 1000 to 1800 cm^{-1}, which contains the most important band regions, amide I, amide II, and amide III.

capacity of the temporary silk−water structure that forms is very unstable and unpredictable. This heat capacity may largely depend on the complicated process of the water loss in different samples under different heating conditions.

For the quickly heated samples (a) and (b) in Figure 1, silk may first form a new structure using water as a plasticizer. For the slowly heated samples (c) and (d) in Figure 1, some bound water molecules transformed to free water molecules and start to evaporate. Meanwhile, other more strongly bound water molecules still act as plasticizers to form the silk−water structure as shown in Figure 2. All of the bound water molecules were finally evaporated around 155 °C. The specific reversing heat capacity in Figure 2 all matched the pure silk fibroin solid baseline at around 160 °C. Subsequently, the stable glass transition of the pure silk fibroin ($T_g(2)$) occurred, and the β-sheet crystals formed after this. With the help of the solid and liquid pure silk baselines, we clearly find that the heat capacity increments of the two samples fit perfectly to the upper (liquid) and lower (solid) baselines, which indicates that these two samples are in the noncrystalline state at 165 °C. At 178 °C, they go through the same glass transition as the repeated "thermal cycles" treated samples in our previous study,[13] in which no water-induced glass transition happened during heating.

This quantitative TMDSC study gives us a clearer picture about what happens when the bound water plasticizer induces a new glass transition in the silk−water system and how this structure transforms to the dry solid state of silk with the loss of the water molecules. Thus, we can conclude that the large endothermic peak seen in the standard DSC trace is due to the heat absorbed by the evaporated water molecules as well as the heat of transformation of the bound water−silk structure to the dry silk structure. Therefore, it is not helpful to integrate the heat flow area of this large endothermic peak and assign it to only one part of this contribution, as was reported in previous work.[5,20] However, TMDSC does not provide complete knowledge about the role of water in this process because thermal analysis cannot tell us what type of structure is formed. Some questions still remain, for example: what is the conformation of this water induced structure? Is it related to the β-sheet crystals? Does the transformation of this structure make the silk chains relax or become more tightly organized? Therefore, FTIR was used to help answer these questions.

Fourier Transform Infrared Spectroscopy. Figure 3 shows a typical FTIR spectrum during a heating from 65 to 165 °C with a heating rate of 2 K/min. The collection time for each spectrum was 63 s. The temperature can be related to time by monitoring the end time of the generation of each spectrum. The frequency is shown from 1000 to 1800 cm^{-1}, which contains the most important band regions of amide I, amide II, and amide III.[48–50] The IR spectral region within 1700−1500 cm^{-1} was assigned to the peptide backbone of amide I (1700−1600 cm^{-1}) and amide II (1600−1500 cm^{-1}) absorptions; the amide III region was from 1350 to 1200 cm^{-1}.[27,28] The amide I region mainly comes from the C═O stretching vibration (80%) with minor contributions from the NH in-plane bending, the out-of-phase CN stretching vibration, and the CCN deformation.[1,24,28] Therefore, the amide I vibration directly depends on the secondary structure of the protein backbone and is most commonly used for the quantitative analysis of different secondary structures. The amide II region is caused mainly by the CN stretching and the NH in-plane bending vibrations of the backbone.[27,28]

Amide I and II Regions. The amide I and II regions are illustrated in parts a and b of Figure 4 for the noncrystallization heating and isothermal crystallization stages, respectively. Figure 4a shows the FTIR spectra in the amide I and II regions of noncrystalline silk fibroin, during heating at 2 K/min, from 65 °C (red trace) to 165 °C (blue trace). The difference, or residual absorbance, between the fibroin spectra at temperature, T, and the spectrum at 65 °C was calculated and is shown in Figure 4c (black or blue traces). In addition to the noncrystalline silk fibroin sample, the control sample of silk treated by exposure to MeOH was also scanned under the same conditions. Silk treated by exposure to MeOH contains a large fraction of β-pleated sheets and has no thermal transitions in this range of

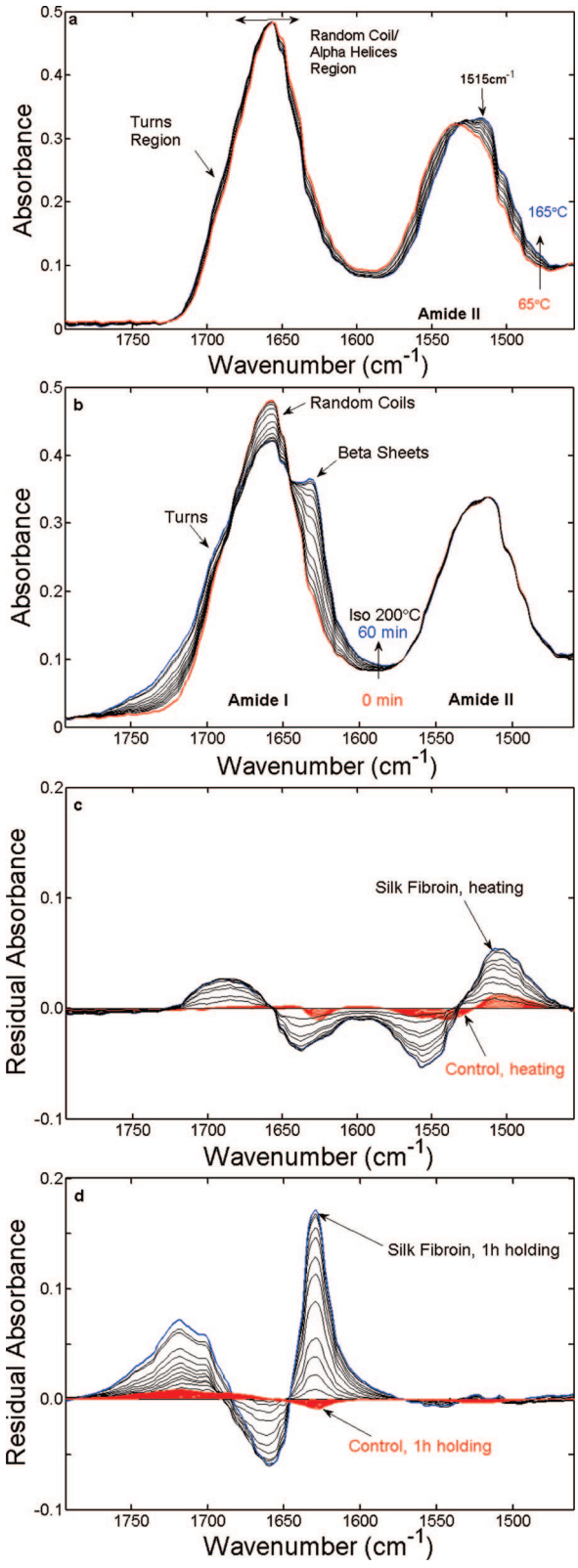

Figure 4. Selected FTIR spectra of silk fibroin film in the amide I and II regions. (a, b) Absorbance vs frequency of noncrystalline silk fibroin: (a) during heating from $T = 65$ °C (red trace) to $T = 165$ °C (blue trace); (b) during isothermal holding at 200 °C for times from $t = 0$ min (red trace) to $t = 60$ min (blue trace). (c, d) Residual absorbance vs frequency: (c) during heating from $T = 65$ °C to $T = 165$ °C for noncrystalline silk fibroin (black traces for $T < 165$ °C; blue trace, $T = 165$ °C) and for MeOH-treated control (red traces); (d) during isothermal holding at 200 °C for times from $t = 0$ min to $t = 60$ min for noncrystalline silk fibroin (black traces, $t < 60$ min; blue trace, $t = 60$ min) and for MeOH-treated control (red traces). The band at 1515 cm^{-1} is marked with an arrow.

temperature. This control was used to illustrate the effect of temperature alone, on a sample whose structure was not changing during the scans. The residual absorbance for the control MeOH-treated silk fibroin sample is shown in Figure 4c (red traces). Generally, an upshift of the amide I region and a downshift of the amide II region were observed during the heating process, which might be related to loss of bound water.

The noncrystallization heating treatment generated a shift to lower frequency of the amide II region, and a small increase in absorbance at 1515 cm^{-1}, in the noncrystalline sample. When this sample is cooled to room temperature, the changes observed at 165 °C remain as permanent features and are much larger in the noncrystalline sample than in the control. Within the amide II frequency region, a small peak appears at 1515 cm^{-1}. The peak at 1515 cm^{-1} in the IR spectrum of silk fibroin (marked by an arrow in Figure 4a) has been observed and discussed by many researchers.[7,39,51–53] It has been assigned to the ring CC stretching and CH bending mode of the tyrosine (Tyr) side chain.[54,55] Earlier studies all showed that crystallized silk fibroin samples change significantly in the 1600−1500 cm^{-1} region, compared with the noncrystalline silk fibroin samples, regardless of whether they were in the solid state or solution state. The most obvious feature in this change was the appearance of the band at 1515 cm^{-1}. Previously, during fast crystallization of silk, the change of 1600−1500 cm^{-1} region and the small peak at 1515 cm^{-1} could not be separated from the process of β-sheet formation, when observed directly from an IR spectrum taken after the *completion* of crystallization.[7,39] Therefore, for a long time, changes in the 1515 cm^{-1} region were always taken as an additional sign for β-sheets crystallization of silk fibroin, similar to the change of the 1620 cm^{-1} band in the amide I region. In our work reported here, the silk sample takes a longer time to reach the starting point for crystallization, which is above T_g (178 °C). Our results show that the small peak at 1515 cm^{-1} has completely changed *before* the silk sample ever reached the crystallization temperature. During heating from 65 to 165 °C, the amide II region shifted to lower frequency, and the small peak at 1515 cm^{-1} gradually increased. Meanwhile, in the amide I region there was no obvious increase in the signature β-sheets peak at 1620 cm^{-1}.

Barth et al.[27,28] completely mapped the effect of the vibrational modes of protein side chain groups to their IR spectrum in the amide II frequency region. The band at 1515 cm^{-1} was attributed to different vibrational modes of Tyr side chains.[27,28,31,53–56] *B. mori* silk fibroin contains 4.8% Tyr, although its main components are Ala (30%), Gly (42.9%), and Ser (12.2%).[12] The majority of the Tyr amino acids contribute at the interfaces of the β-sheet regions (Ala -Gly-Ala-Ser) and act as turns, according to the model from Hudson et al.[16] Fabian and Naumann et al.[31,32,34,35,53] studied the C−C aromatic ring stretching vibration of the Tyr side chain at 1515 cm^{-1} and indicated that this band provided a specific local monitor for the conformational changes, due to reduction of the conformational freedom in the protein structure. According to the studies of small protein RNases and their similar derivatives by Fabian et al.,[31,32,34,35,53] an absorbance change in the Tyr band was observed when hydrophobic cores of a protein are formed, when solvent molecules are excluded from the vicinity of Tyr residues that are buried in native protein molecule. Murayama et al.[33] observed this phenomenon also, in the study of bovine serum albumin (BSA). In silk fibroin film, the situation could be similar, with the small shift and increase in the 1515 cm^{-1} reflecting a reduction of conformational freedom as water is removed during heating. To investigate more fully the role of water removal on the amide II region and on the Tyr side chains, future experiments should be conducted with deuterated samples.

In contrast to the result of Figure 4a,c during heating to 165 °C, the FTIR spectrum of silk fibroin film isothermally crystallized at 200 °C was determined. To avoid crystallization before reaching 200 °C, the hot stage was programmed to jump the temperature from 165 to 200 °C in less than 5 s. Figure 4b shows the spectra in the amide I and II regions for initially noncrystalline silk fibroin, from 0 min (red trace) to 60 min (blue trace) during isothermal holding. The MeOH-treated silk fibroin control was also subject to the same holding treatment for comparison. Residual absorbance between the spectra at time, t, and the spectrum at $t = 0$ (start of isothermal period) are presented in Figure 4d, for both MeOH-treated silk fibroin control (red traces) and initially noncrystalline fibroin (black and blue traces). The amide I region, due mainly to stretching vibrations, experienced a significant transformation. The region from 1600 to 1640 cm^{-1} generates a strong peak, centered at 1625 cm^{-1}, the region from 1640 to 1660 cm^{-1} largely decreases at the same time, and a small increase occurs in the region from 1690 to 1750 cm^{-1}. We have quantitatively discussed in our previous work[1] that the amide I region can accurately show the amount of secondary structure in the protein by comparison with DSC results. All bands in the amide I region could be assigned according to the literature. The region from 1600 to 1640 cm^{-1} arises from β-sheets, which increased during isothermal crystallization and contributed to the major increase in the amide I region. The region from 1640 to 1660 cm^{-1} included contributions from random coils and α-helix structures in the silk fibroin, and these decreased and transformed to the β-sheet crystal structure during crystallization.[1] The remaining part of the amide I region from 1660 to 1690 cm^{-1} arose mainly from the turns and remained relatively stable during crystallization.

During isothermal crystallization, no major change was observed in the amide II region. In general, the crystallization spectra of silk fibroin in the amide I and II regions are quite different compared to the noncrystallization heating spectra (Figure 4a) below the glass transition temperature. During crystallization, shown in Figure 4b, the conformation of the silk secondary structure was largely changed during the formation of β-sheet hydrogen bonds. Therefore, the major change during crystallization occurred in amide I, the C═O stretching region. Next, we examine the amide III region during the noncrystallization heating and the isothermal crystallization.

Amide III Region. By analyzing the protein spectrum amide III region whose structures are already known from other methods or by analyzing model peptides, the bands in the amide III region (1200−1350 cm^{-1}) can be assigned to different secondary structures.[57–61] According to the results from Singh et al.,[57–59] the maximum absorbance for the α-helix is around 1300 cm^{-1}, while β-sheet (range 1200−1240 cm^{-1}) is around 1235 cm^{-1}. The band for pure turn structure was around 1260−1280 cm^{-1}, whereas for the random coil the band was located around 1240−1260 cm^{-1}. Figure 5a shows the FTIR spectrum of silk fibroin film in the amide III region (1200−1350 cm^{-1}) during noncrystallization heating from 65 °C (red trace) to 165 °C (blue trace). An obvious spectral change occurred during the noncrystallization heating process. The peak centered at 1230 cm^{-1} shifted to 1215 cm^{-1}. According to the the amide III region assignment of Singh et al.,[57–59] this peak shift refers to the β-sheet region (1200−1240 cm^{-1}). The difference spectra are shown in Figure 5c (black or blue traces), compared with the MeOH treated control silk sample (red traces) scanned under the same conditions.

Some researchers speculated that there are more α-helical structures formed before the crystallization of silk in their study of silk solutions.[62] However, there were no other major changes in our film study occurring in the amide I and III regions before crystallization, even though the amide III region is particularly well suited to separate the α-helix region (1280−1320 cm^{-1}) from other secondary structures, for example, random coils. No obvious changes occurred in the α-helix region during heating. In a recent NMR study,[63,64] it was suggested that the β-helix or distorted β-turns structures may exist as an intermediate during the formation of the crystals in silk fibroin.

In comparison to the spectra during heating to 165 °C (Figure 5a), Figure 5b shows the FTIR spectrum of silk fibroin in the amide III region during isothermal crystallization at 200 °C from 0 min (red trace) to 60 min (blue trace). With time, the amide III region went through a change in the secondary structural regions. In the β-sheet-related region (1200−1240 cm^{-1}), only a slight shift was seen. In the random coil (1240−1260 cm^{-1}) and α-helix (1280−1320 cm^{-1}) regions, during isothermal crystallization, the band absorbance drops gradually, which indicates change of these structures in the region relating to the NH bending mode. This result was compatible with the decrease of random coil and α-helix absorbance in the amide I region from 1640 to 1660 cm^{-1}. The difference spectra are shown in Figure 5d (black or blue traces), compared with the MeOH treated control silk sample (red traces).

In the 1980s, when silk was first detailed by FTIR spectroscopy, Nadiger, et al. found that a new peak at 1260 cm^{-1} appeared in crystallized silk samples.[65,66] Combined with the peak at 1230 cm^{-1}, they concluded that 1260 cm^{-1} was one of the silk β-sheet peaks in the FTIR spectrum. Then a method to calculate the silk crystallinity based on the absorbance strength ratio of I_{1260}/I_{1230} or $I_{1260}/(I_{1230} + I_{1260})$ was developed and still is used by many researchers today.[51,67–69] Our spectra (Figure 5b) reveal that the shoulder/peak at 1260 cm^{-1} appears as a result of a *decrease* of the absorbance on the left and right sides and not as a result of increase of the absorbance at 1260 cm^{-1}. This conclusion is borne out by observation of the residual absorbance spectra, shown in Figure 5d. Therefore, the apparent "peak" at 1260 cm^{-1} might actually be better assigned to the turns structure, an assignment which is similar to other proteins.[57–59] The prior method for calculating the β-sheets crystallinity[51,65–69] should be reconsidered to account for this new observation. We have provided two alternate methods to calculate the crystallinity for the silk fibroin film by using FTIR and DSC, and they can be combined together for a high level of accuracy.[1,13] Therefore, we recommend in the study of silk that these two methods be used for the absolute calculation of crystallinity in silk fibroin samples.

Comparison with Synthetic Polymer Crystallization. An analogy can be made in the present case between the natural silk biopolymer crystallization process and that of synthetic polymers depicted in Figure 6a,b. Recently, Strobl has presented a description for the sequence of melt crystallization of synthetic polymers, using a four-state scheme.[70,71] In the four-state scheme, the synthetic polymer amorphous melt first organizes into a mesophase, from which granular crystal blocks, and then chain-folded crystal lamellae, grow.

The mesophase is described as being similar to a "fluid hexatic phase"[71] whose order is intermediate between that of the fully isotropic melt and the three-dimensionally ordered crystal. Figure 6a is adapted from Strobl's sketch[71] in which the sequence of crystallization starts from the melt (1), through a mesomorphic layer (2), to a granular crystal layer (3), and thence to lamellar crystal (4). The intermediate degree of ordering of the mesophase is such that adjacent chains have chain direction aligned more nearly parallel, while not yet as ordered as the three-dimensional crystalline lamellae. The mesophase has less mobility than the unconstrained amorphous melt.

In the present study of natural silk biopolymer, we suggest that the progression of β-sheet crystal formation likewise may

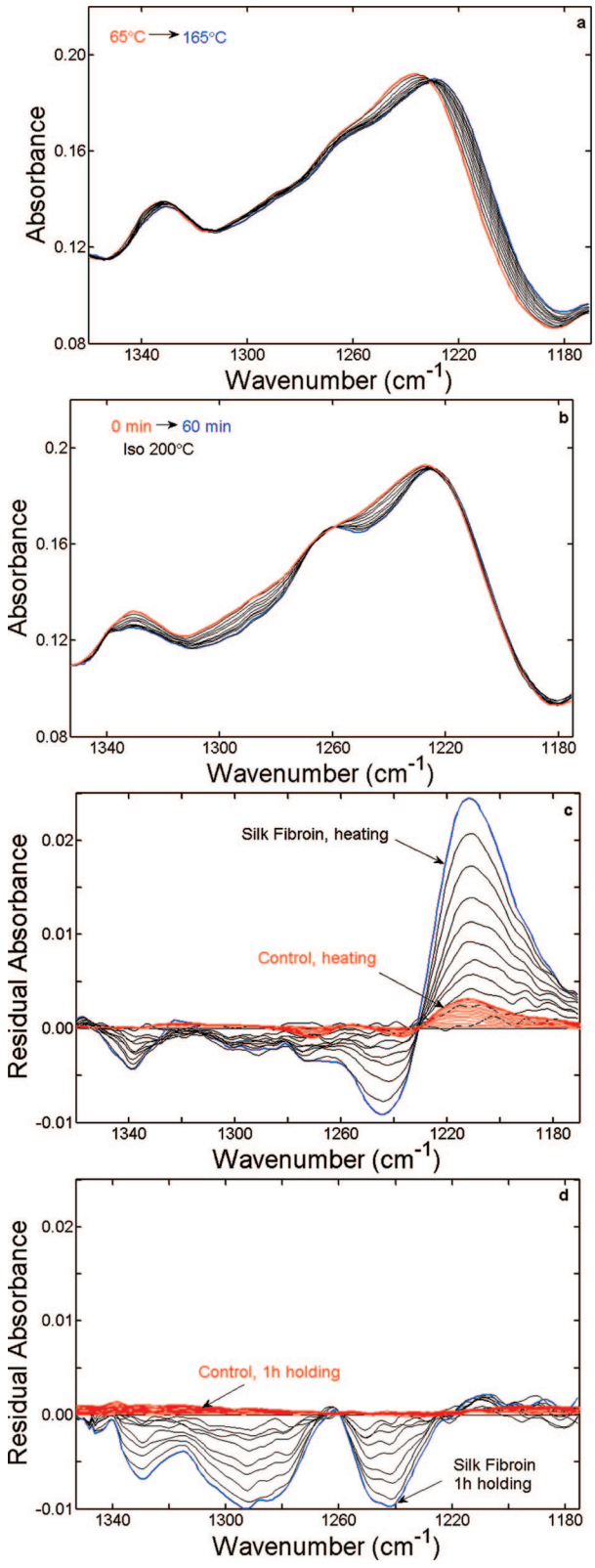

Figure 5. Selected FTIR spectra of silk fibroin film in the amide III (1200−1350 cm^{-1}) region: (a, b) Absorbance vs frequency of noncrystalline silk fibroin: (a) during heating from $T = 65$ °C (red trace) to $T = 165$ °C (blue trace); (b) during isothermal holding at 200 °C for times from $t = 0$ min (red trace) to $t = 60$ min (blue trace). (c, d) Residual absorbance vs frequency: (c) during heating from $T = 65$ °C to $T = 165$ °C for noncrystalline silk fibroin (black traces for $T <$ 165 °C; blue trace, $T = 165$ °C) and for MeOH-treated control (red traces); (d) during isothermal holding at 200 °C for times from $t = 0$ min to $t = 60$ min for noncrystalline silk fibroin (black traces, $t < 60$ min; blue trace, $t = 60$ min) and for MeOH-treated control (red traces).

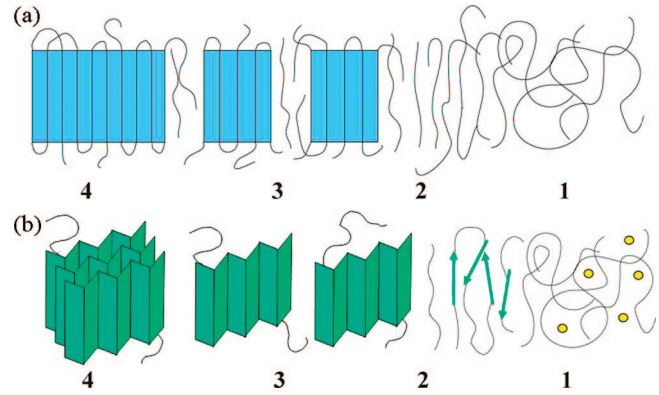

Figure 6. (a) Formation of lamellar stacks via mesophase formation, drawn according to the model proposed by Strobl for synthetic polymers:[71] 1, amorphous melt; 2, mesophase; 3, granular crystal blocks; 4, lamellar crystal. (b) Suggested corresponding formation of stacked β-pleated sheet crystals in fibrous proteins via precursor formation: 1, system of protein + bound water (bound water, yellow circles) below $T_g(1)$ in random coil structure; 2, precursor structure below $T_g(2)$ after removal of bound water (β-strands, green arrows); 3, β-pleated sheets above $T_g(2)$; 4, stacked β-pleated sheet crystal. In parts 1 and 2, the phenyl ring icon designates the Tyr side group. These are omitted from parts 3 and 4.

proceed from a disordered noncrystalline state (of random coils and α-helices) containing bound water (Figure 6b, state 1), to a precursor state (state 2) of higher molecular chain order following removal of bound water, to the formation of single β-pleated sheets (state 3), and finally to the formation of three-dimensional β-pleated sheet crystals (state 4).

With bound water molecules acting as a plasticizer (Figure 6b, state 1), the silk−water structure has a glass transition temperature, $T_g(1)$, lower than that of the dry silk, $T_g(2)$, (as indicated in Figures 1 and 2). Our heat capacity results demonstrate that above this glass transition temperature silk fibroin chains obtain sufficient mobility to form an unstable structure with bound water molecules. This unstable structure is not the final β-pleated-sheet crystal structure of silk fibroin but is an aggregated structure that includes bound water molecules. Further increase of temperature causes loss of the bound water molecules, which are excluded from the newly formed silk structure (Figure 6b, state 2) in which the bulky Tyr side groups are located away from the β-strand regions.[16] After water removal, the silk fibroin chain structure will not transform back to its original less dense structure. The chains remain in this denser, solid (but noncrystalline) structure finally forming hydrophobic cores (Figure 6b, state 2). These structures may be similar to the intermediate distorted β-turn structures suggested in an NMR study of fibroin.[63,64]

This new pure silk structure has a slightly different secondary structure compared with the original water-containing structure and may promote the formation of the stacked β-pleated-sheet crystal more easily, although (as shown in Figure 4a,c) this structure itself has no β-pleated-sheet crystals. This hypothesized solid-state silk precursor structure may be important for preparing the crystallization of the silk fibroin and could be analogous to the native process in the worm. After the formation of this precursor structure, our heat capacity (Figure 2) shows that the glass transition of the pure silk fibroin, $T_g(2)$ (178 °C), occurs immediately after a short increase of temperature. The inter- or intramolecular β-pleated-sheet crystals are then successfully generated from the silk fibroin structure (Figure 6b, state 3) by a process similar to cold crystallization of synthetic polymer.[1] In the final step, the β-pleated sheets crystallize into stacked three-dimensional β-sheet crystals (Figure 6b, state 4), as shown by X-ray scattering and thermal analysis.[72]

The precursor structure may possibly be like the silk I structure within the gland of silkworms before spinning silk fibers, which structure has been measured in the dried state.[12,22,73–76] This suggestion successfully explains the important role of water molecules during the crystallization of the silk fibroin. The authors believe that this slow thermal crystallization process in silk fibroin film is fundamentally similar to the fast crystallization process of silk fibers when they are spun out from the silkworm spinner and transformed from silk I to silk II.

However, the mechanism of the crystallization of β-sheet protein is not fully like that of melt crystallization proposed by Strobl[70,71] for common thermoplastic semicrystalline polymers. First, thermoplastic polymers can crystallize either from the melt or from the glassy state in the absence of solvent molecules. But for silk fibroin the formation of the precursor structure is largely dependent on the function of the bound water molecules. Second, melt-crystallized polymers return to the amorphous molten state when they are heated above their crystallization temperatures, whereas silk fibroin β-sheet crystals degrade before they melt.

Conclusion

This study provides a clearer picture of how silk fibroin chains can self-assemble from the noncrystalline, water-soluble structure to the β-sheet-crystal rich insoluble final structure. The fundamental mechanism is the role of the water molecules. DSC study shows that silk fibroin displays a water-induced glass transition around 80 °C during quick heating, resulting from a temporary bound water−silk structure. Quantitative thermal analysis of the heat capacity changes of this system during heating confirmed the plasticization of silk by water but revealed that no β-sheets crystal were formed during the heating process below $T_g(2)$. FTIR study shows the amide II region and the 1515 cm^{-1} band are both affected by water removal during heating below T_g. This may indicate a change of the microenvironment in the silk fibroin chains caused by bound water molecules. During isothermal crystallization above $T_g(2)$ the silk fibroin amide I spectra showed a phase transition from the secondary structures of noncrystalline random coils and α-helices to β-pleated-sheet crystals, while the amide II region remained stable during this process.

This study also provides two important techniques for the study of the effects of water on polymers. TMDSC can be used to separate the nonreversing water evaporation process from the reversing glass transition of the water−polymer system. In addition, the quantitative heat capacity study of the water−polymer system will reveal whether the water-induced structure can effect crystallization of the polymer immediately or, as in the present case, the heat capacity returns to the baseline noncrystalline solid below $T_g(2)$. On the other hand, temperature-dependent FTIR provides information about the changing vibrational bands during temperature ramping. The change from the water-induced structure and the process of crystallization can be shown in the specific amide band regions. The protein structure can be examined in detail by this method. All of these applications will help in the study of macromolecular science (especially biopolymer and food science) to understand more deeply the function of water molecules in a polymer system.

Acknowledgment. s thank the National Science Foundation for support of this work through the Polymers Program of the Division of Materials Research under DMR-0402849 and the MRI Program for thermal analysis instrumentation under DMR-0520655. D.K. also acknowledges the Air Force Office of Scientific Research for partial support through grant FA-9550-07-1-0079. Helpful discussions with Dr. Regina Valluzzi are acknowledged.

References and Notes

(1) Hu, X.; Kaplan, D.; Cebe, P. *Macromolecules* **2006**, *39*, 6161–6170.
(2) Pyda, M. *Macromolecules* **2002**, *35*, 4009–4016.
(3) Pyda, M. *J. Polym. Sci., Part B: Polym. Phys.* **2001**, *39*, 3038–3054.
(4) Hodge, R. M.; Bastow, T. J.; Edward, G. H.; Simon, G. P.; Hill, A. J. *Macromolecules* **1996**, *29*, 8137–8143.
(5) Kim, Y. S.; Dong, L. M.; Hickner, M. A.; Glass, T. E.; Webb, V.; McGrath, J. E. *Macromolecules* **2003**, *36*, 6281–6285.
(6) Agarwal, N.; Hoagland, D. A.; Farris, R. J. *J. Appl. Polym. Sci.* **1997**, *63*, 401–410.
(7) Min, B. M.; Jeong, L.; Lee, K. Y.; Park, W. H. *Macromol. Biosci.* **2006**, *6*, 285–292.
(8) Lee, K. Y.; Ha, W. S. *Polymer* **1999**, *40*, 4131–4134.
(9) Slade, L.; Levine, H. *J. Food Eng.* **1995**, *24*, 431–509.
(10) Doster, W.; Settles, M. *Biochim. Biophys. Acta* **2005**, *1749*, 173–186.
(11) Lin, S. Y.; Chu, H. L. *Int. J. Biol. Macromol.* **2003**, *32*, 173–177.
(12) McGrath, K., Kaplan, D., Eds.; *Protein-Based Materials*; Birkhauser Press: Boston, 1996; pp 103−133.
(13) Hu, X.; Kaplan, D.; Cebe, P. *Thermochim. Acta* **2007**, *461* (1−2), 137–144.
(14) Altman, G. H.; Diaz, F.; Jakuba, C.; Calabro, T.; Horan, R. L.; Chen, J. S.; Lu, H.; Richmond, J.; Kaplan, D. L. *Biomaterials* **2003**, *24*, 401–416.
(15) Foo, C. W. P.; Kaplan, D. L. *Adv. Drug Delivery Rev.* **2002**, *54*, 1131–1143.
(16) Ha, S. W.; Gracz, H. S.; Tonelli, A. E.; Hudson, S. M. *Biomacromolecules* **2005**, *6*, 2563–2569.
(17) Chen, X.; Zhou, L.; Shao, Z. Z.; Zhou, P.; Knight, D. P.; Vollrath, F. *Acta Chim. Sin.* **2003**, *61*, 625–629.
(18) Ishida, M.; Asakura, T.; Yokoi, M.; Saito, H. *Macromolecules* **1990**, *23*, 88–94.
(19) Chen, X.; Shao, Z. Z.; Marinkovic, N. S.; Miller, L. M.; Zhou, P.; Chance, M. R. *Biophys. Chem.* **2001**, *89*, 25–34.
(20) Motta, A.; Fambri, L.; Migliaresi, C. *Macromol. Chem. Phys.* **2002**, *203*, 1658–1665.
(21) Tretinnikov, O. N.; Tamada, Y. *Langmuir* **2001**, *17*, 7406–7413.
(22) Jin, H. J.; Kaplan, D. L. *Nature (London)* **2003**, *424*, 1057–1061.
(23) Magoshi, J.; Magoshi, Y.; Nakamura, S.; Kasai, N.; Kakudo, M. *J. Polym. Sci., Part B: Polym. Phys.* **1977**, *15*, 1675–1683.
(24) Goormaghtigh, E.; Cabiaux, V.; Ruysschaert, J. M. *Eur. J. Biochem.* **1990**, *193*, 409–420.
(25) Jung, C. *J. Mol. Recognit.* **2000**, *13*, 325–351.
(26) Dong, A.; Huang, P.; Caughey, W. S. *Biochemistry* **1990**, *29*, 3303–3308.
(27) Barth, A. *Prog. Biophys. Mol. Biol.* **2000**, *74*, 141–173.
(28) Barth, A.; Zscherp, C. *Q. Rev. Biophys.* **2002**, *35*, 369–430.
(29) Fabian, H.; Naumann, D. *Methods* **2004**, *34*, 28–40.
(30) Vanstokkum, I. H. M.; Linsdell, H.; Hadden, J. M.; Haris, P. I.; Chapman, D.; Bloemendal, M. *Biochemistry* **1995**, *34*, 10508–10518.
(31) Fabian, H.; Schultz, C.; Backmann, J.; Hahn, U.; Saenger, W.; Mantsch, H. H.; Naumann, D. *Biochemistry* **1994**, *33*, 10725–10730.
(32) Fabian, H.; Schultz, C.; Naumann, D.; Landt, O.; Hahn, U.; Saenger, W. *J. Mol. Biol.* **1993**, *232*, 967–981.
(33) Murayama, K.; Tomida, M. *Biochemistry* **2004**, *43*, 11526–11532.
(34) Backmann, J.; Schultz, C.; Fabian, H.; Hahn, U.; Saenger, W.; Naumann, D. *Proteins: Struct, Funct, Genet.* **1996**, *24*, 379–387.
(35) Reinstadler, D.; Fabian, H.; Backmann, J.; Naumann, D. *Biochemistry* **1996**, *35*, 15822–15830.
(36) Wang, S. L.; Lin, S. Y.; Li, M. J.; Wei, Y. S.; Hsieh, T. F. *Biophys. Chem.* **2005**, *114*, 205–212.
(37) Lin, S. Y.; Hsieh, T. F.; Wei, Y. S. *Peptides* **2005**, *26*, 543–549.
(38) Chen, X.; Shao, Z. Z.; Knight, D. P.; Vollrath, F. *Acta Chim. Sin.* **2002**, *60*, 2203–2208.
(39) Jeong, L.; Lee, K. Y.; Liu, J. W.; Park, W. H. *Int. J. Biol. Macromol.* **2006**, *38*, 140–144.
(40) Ishikiriyama, K.; Wunderlich, B. *J. Therm. Anal.* **1997**, *50*, 337–346.
(41) Wunderlich, B.; Jin, Y. M.; Boller, A. *Thermochim. Acta* **1994**, *238*, 277–293.
(42) Boller, A.; Okazaki, I.; Ishikiriyama, K.; Zhang, G.; Wunderlich, B. *J. Therm. Anal.* **1997**, *49*, 1081–1088.
(43) Xu, H.; Cebe, P. *Macromolecules* **2005**, *38*, 770–779.
(44) Xu, H.; Cebe, P. *Macromolecules* **2004**, *37*, 2797–2806.
(45) Pyda, M.; Boller, A.; Grebowicz, J.; Chuah, H.; Lebedev, B. V.; Wunderlich, B. *J. Polym. Sci., Part B: Polym. Phys.* **1998**, *36*, 2499–2511.
(46) Pyda, M.; Wunderlich, B. *Macromolecules* **1999**, *32*, 2044–2050.
(47) Sugisaki, M.; Suga, H.; Seki, S. *Bull. Chem. Soc. Jpn.* **1968**, *41*, 2591–2599.
(48) Sonoyama, M.; Nakano, T. *Appl. Spectrosc.* **2000**, *54*, 968–973.

(49) Skrovanek, D. J.; Howe, S. E.; Painter, P. C.; Coleman, M. M. *Macromolecules* **1985**, *18*, 1676–1683.
(50) Skrovanek, D. J.; Painter, P. C.; Coleman, M. M. *Macromolecules* **1986**, *19*, 699–705.
(51) Um, I. C.; Kweon, H. Y.; Lee, K. G.; Park, Y. H. *Int. J. Biol. Macromol.* **2003**, *33*, 203–213.
(52) Um, I. C.; Ki, C. S.; Kweon, H. Y.; Lee, K. G.; Ihm, D. W.; Park, Y. H. *Int. J. Biol. Macromol.* **2004**, *34*, 107–119.
(53) Reinstadler, D.; Fabian, H.; Naumann, D. *Proteins: Struct., Funct., Genet.* **1999**, *34*, 303–316.
(54) Venyaminov, S. Yu.; Kalnin, N. N. *Biopolymers* **1990**, *34*, 1259–1271.
(55) Hienerwadel, R.; Boussac, A.; Breton, J.; Diner, B. A.; Berthomieu, C. *Biochemistry* **1997**, *36*, 14712–14723.
(56) Venyaminov, S. Y.; Kalnin, N. N. *Biopolymers* **1990**, *30*, 1243–1257.
(57) Cai, S. W.; Singh, B. R. *Biophys. Chem.* **1999**, *80*, 7–20.
(58) Fu, F. N.; Deoliveira, D. B.; Trumble, W. R.; Sarkar, H. K.; Singh, B. R. *Appl. Spectrosc.* **1994**, *48*, 1432–1441.
(59) Cai, S. W.; Singh, B. R. *Biochemistry* **2004**, *43*, 2541–2549.
(60) Mikhonin, A. V.; Asher, S. A. *J. Am. Chem. Soc.* **2006**, *128*, 13789–13795.
(61) Mikhonin, A. V.; Bykov, S. V.; Myshakina, N. S.; Asher, S. A. *J. Phys. Chem. B* **2006**, *110*, 1928–1943.
(62) Drummy, L. F.; Phillips, D. M.; Stone, M. O.; Farmer, B. L.; Naik, R. R. *Biomacromolecules* **2005**, *6*, 3328–3333.
(63) Yamane, T.; Umemura, K.; Nakazawa, Y.; Asakura, T. *Macromolecules* **2003**, *36*, 6766–6772.
(64) Lazo, N. D.; Downing, D. T. *Macromolecules* **1999**, *32*, 4700–4705.
(65) Bhat, N. V.; Nadiger, G. S. *J. Appl. Polym. Sci.* **1980**, *25*, 921–932.
(66) Nadiger, G. S.; Halliyal, V. G. *Colourage* **1984**, *31*, 23–32.
(67) Shao, J. Z.; Zheng, J. H.; Liu, J. Q.; Carr, C. M. *J. Appl. Polym. Sci.* **2005**, *96*, 1999–2004.
(68) Lv, H. Q.; Feng, Y. L.; Zhang, S. X.; Guo, J. Z. *Mater. Lett.* **2005**, *59*, 3109–3111.
(69) Um, I. C.; Kweon, H. Y.; Park, Y. H.; Hudson, S. *Int. J. Biol. Macromol.* **2001**, *29*, 91–97.
(70) Schmidtke, J.; Strobl, G.; ThurnAlbrecht, T. *Macromolecules* **1997**, *30*, 5804–5821.
(71) Strobl, G. *Eur. Phys. J. E* **2000**, *3*, 165.
(72) Hu, X.; Cebe, P. *Proc. Am. Chem. Soc., Div. Polym. Mater.: Sci. Eng.* **2005**, *93*, 652–653.
(73) Valluzzi, R.; Jin, H. J. *Biomacromolecules* **2004**, *5*, 696–703.
(74) Valluzzi, R.; Szela, S.; Avtges, P.; Kirschner, D.; Kaplan, D. *J. Phys. Chem. B* **1999**, *103*, 11382–11392.
(75) Monti, P.; Freddi, G.; Bertoluzza, A.; Kasai, N.; Tsukada, M. *J. Raman Spectrosc.* **1998**, *29*, 297–304.
(76) Kaplan, D. L., Adams, W. W., Farmer, B., Viney, C., Eds.; *Silk Polymers: Materials Science and Biotechnology*; ACS Symposium Series 544; American Chemical Society: Washington, DC, 1994.

MA071551D